Titel/Title: Beating Thermal Coarsening in Nanoporous Materials via High-Entropy Design

Autor*innen/Author(s): Soo-Hyun Joo, Jae Wung Bae, Won-Young Park, Yusuke Shimada, Takeshi Wada, Hyoung Seop Kim, Akira Takeuchi, Toyohiko J. Konno, Hidemi Kato, Ilya V. Okulov

Veröffentlichungsversion/Published version: Postprint

Publikationsform/Type of publication: Artikel/Aufsatz

Empfohlene Zitierung/Recommended citation:

Joo, S.-H., Bae, J. W., Park, W.-Y., Shimada, Y., Wada, T., Kim, H. S., Takeuchi, A., Konno, T. J., Kato, H., Okulov, I. V., Beating Thermal Coarsening in Nanoporous Materials via High-Entropy Design. Adv. Mater. 2020, 32, 1906160. https://doi.org/10.1002/adma.201906160

Verfügbar unter/Available at:
(wenn vorhanden, bitte den DOI angeben/please provide the DOI if available)

https://doi.org/10.1002/adma.201906160

Zusätzliche Informationen/Additional information:

Beating Thermal Coarsening in Nanoporous Materials via High-Entropy Design

Soo-Hyun Joo, Jae Wung Bae, Won-Young Park, Yusuke Shimada, Takeshi Wada, Hyoung Seop Kim, Akira Takeuchi, Toyohiko J. Konno, Hidemi Kato,* and Ilya V. Okulov*

Controlling the feature sizes of 3D bicontinuous nanoporous (3DNP) materials is essential for their advanced applications in catalysis, sensing, energy systems, etc., requiring high specific surface area. However, the intrinsic coarsening of nanoporous materials naturally reduces their surface energy leading to the deterioration of physical properties over time, even at ambient temperatures. A novel 3DNP material beating the universal relationship of thermal coarsening is reported via high-entropy alloy (HEA) design. In newly developed TiVNbMoTa 3DNP HEAs, the nanoporous structure is constructed by very fine nanoscale ligaments of a solid-solution phase due to enhanced phase stability by maximizing the configuration entropy and suppressed surface diffusion. The smallest size of 3DNP HEA synthesized at 873 K is about 10 nm, which is one order of magnitude smaller than that of conventional porous materials. More importantly, the yield strength of ligament in 3DNP HEA approaches its theoretical strength of $G/2\pi$ of the corresponding HEA alloy even after thermal exposure. This finding signifies the key benefit of high-entropy design in nanoporous materials—exceptional stability of size-related physical properties. This high-entropy strategy should thus open new opportunities for developing ultrastable nanomaterials against its environment.

Stabilizing the feature sizes of 3D bicontinuous nanoporous (3DNP) is technically challenging because the coarsening follows a universal empirical correlation with homologous temperature ($T_{\text{melting point}}/T_{\text{dealloying or annealing}}$): their mature ligament size is inversely proportional to the melting point.[1,2] Ligament coarsening is a surface-diffusion-dominated process, and the relationship between the melting point and diffusion is apparent in solid solutions. Although 3DNP materials produced by dealloying have outstanding physical properties due to their unique structure with open porous networks,[3–5] the undesirable coarsening phenomenon leads to degradation of physical properties over time, even at room temperature.[6–8]

The originally proposed idea behind high-entropy alloy (HEA) with multiprinciple elements is maximizing the configuration entropy to stabilize a solid-solution alloy without undesired ordered intermetallics.[9–11] Many studies have suggested that HEAs uniquely possesses combined desirable properties such as a high strength and ductility paired with high fracture toughness,[12–14] fatigue resistance,[15] and creep resistance.[16] HEAs also show promising properties in harsh environments resisting corrosion,[17–19] and irradiation[20] attacks. Atomic size differences between constituting elements in HEA increase the activation energy for grain growth, and sluggish diffusion kinetics has considered as the main reason for the exceptional high strength and structural stability of HEAs at high temperatures.[21,22] The rationale behind it, the multiprinciple elements cause larger fluctuations in lattice potential energy (LPE), providing many low-LPE sites that hinder atomic diffusion.[23] Grain growth and ligament coarsening rely on the same physical background of surface diffusion. In that context, the high-entropy design in nanoporous materials has a potential for achieving an exceptional stability against the coarsening.

Prof. S.-H. Joo, Dr. W.-Y. Park, Prof. Y. Shimada, Prof. T. Wada, Prof. T. J. Konno, Prof. H. Kato, Dr. I. V. Okulov
Institute for Materials Research
Tohoku University
Katahira 2-1-1, Sendai 980-8577, Japan
E-mail: jjsh83@imr.tohoku.ac.jp; hikato@imr.tohoku.ac.jp

Dr. J. W. Bae, Prof. H. S. Kim
Department of Materials Science and Engineering
Pohang University of Science and Technology
77 Cheongam-Ro, Pohang 37673, South Korea

Prof. A. Takeuchi
Graduate School of Engineering
Tohoku University
Aoba-ku 6-6-01-2, Sendai 980-8579, Japan

Dr. I. V. Okulov
Faculty of Production Engineering
University of Bremen
Badgasteiner Str. 1, 2, Bremen 8359, Germany

Dr. I. V. Okulov
Leibniz Institute for Materials Engineering – IWT
Badgasteiner Str. 3, Bremen 28359, Germany

Dr. I. V. Okulov
Institute of Natural Sciences and Mathematics
Ural Federal University
Yekaterinburg 620002, Russia

To synthesize the 3DNP HEA, we utilized liquid metal dealloying (LMD), a unique technique to fabricate non-noble porous materials used in structural, functional, and medical products by preventing oxidation in a metallic melt.[24–30] The high-entropy design of LMD based on the enthalpy of mixing is depicted in **Figure 1**a,b. The composition of the 3DNP HEA is carefully established among elements immiscible with the Mg melt, and then the selected TiVNbMoTa HEA is alloyed with 75 at% miscible Ni. While Ni atoms are selectively dissolved during LMD in the Mg melt, the five immiscible elements rearrange their atomic configuration into a bicontinuous structure. Following this new and practical strategy, many LMD systems can be designed to produce various 3DNP HEAs.

The precursor $(TiVNbMoTa)_{25}Ni_{75}$ mainly consists of two face-centered cubic (FCC) solid-solution phases (Figure S1a, Supporting Information). These two parent phases have different chemical compositions, but both FCC phases transform into their respective body-centered cubic (BCC) ligaments after dealloying due to the dissolution of Ni (Figure S1b, Supporting Information). The average ligament size achieved in a unimodal porous structure formed from the parent FCC1 phase is just 10 nm after 10

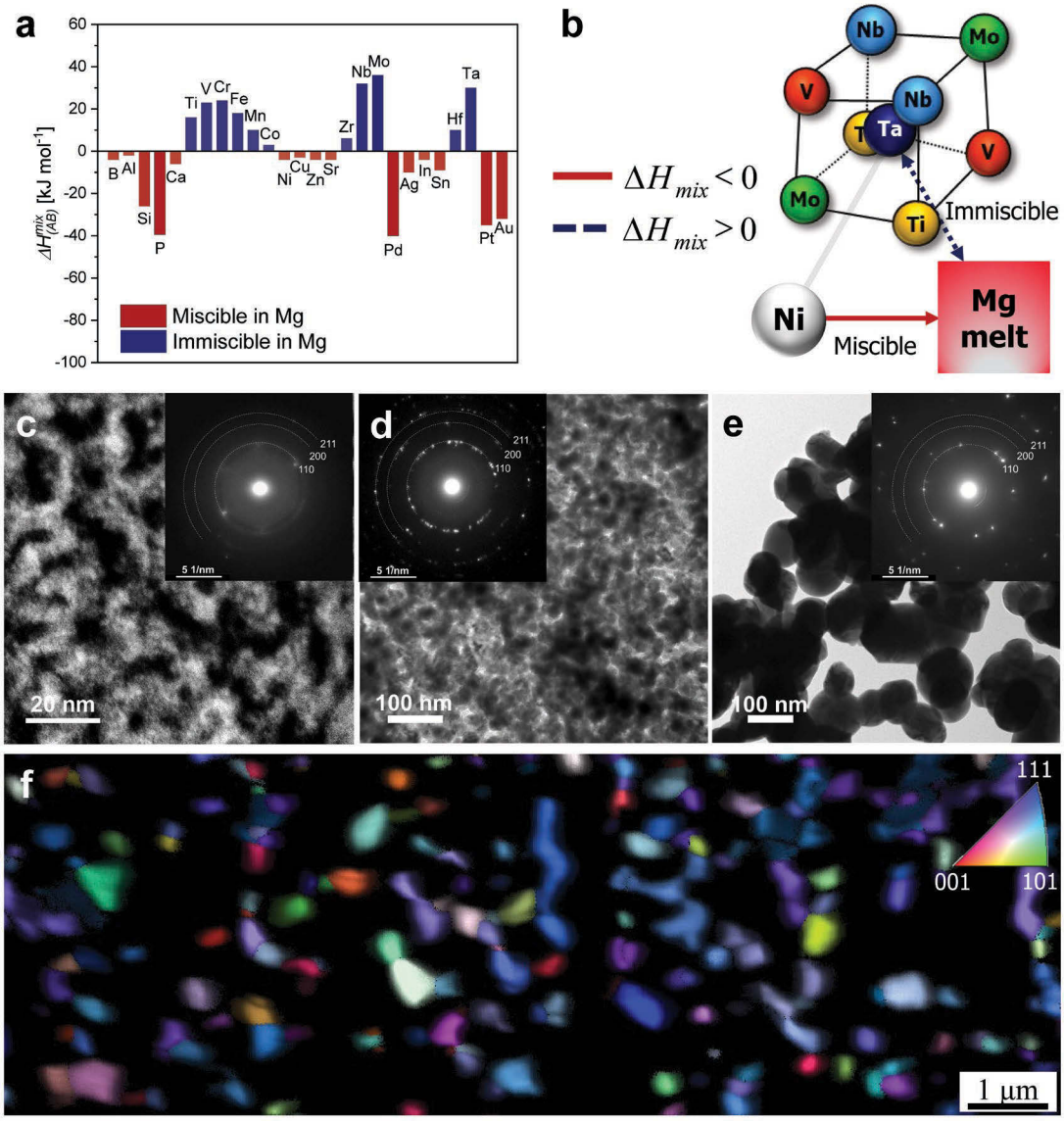

Figure 1. A novel high-entropy design strategy for 3DNP HEA by LMD and the structural evolution of synthesized 3DNP HEAs. a) Enthalpy of mixing between the Mg melt and considered elements. b) Predesigned LMD system based on the miscibility of precursor elements. c) High-angle annular dark-field scanning transmission electron microscopy (HAADF-STEM) image of the 3DNP HEA produced by LMD at 873 K for 10 min. d–e) Bright field (BF) TEM images of the 3DNP HEAs produced at 1073 K for 10 min (d) and for 120 min (e). The selected area diffraction (SAED) patterns in the inset figures show the formation of the BCC structure at all conditions. High-magnification filed emission scanning electron microscope (FE-SEM) images of 3DNP HEAs are presented in Figure S1c–f of the Supporting Information. f) Electron backscatter diffraction (EBSD) inverse pole figure map overlapped on image quality map of the 3DNP HEA produced at 1173 K for 120 min. g) Grain boundary map overlapped on confidence index map corresponding to (g). h) HAADF-STEM image and energy-dispersive X-ray (EDX) maps of the constituent elements in the 3DNP HEA produced at 873 K for 10 min.

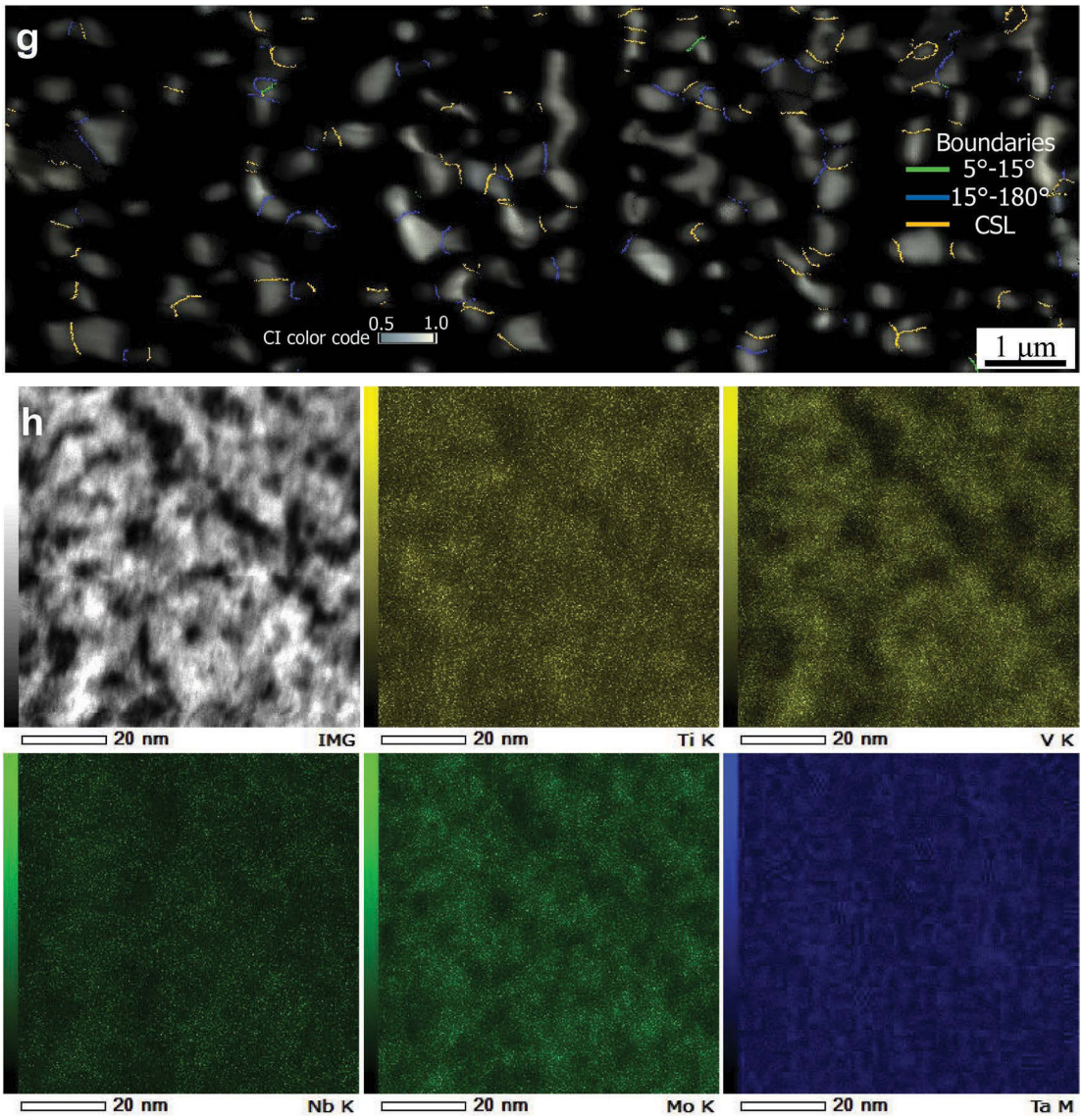

Figure 1. Continued.

(Figure 1c). This is the smallest ligament size ever reported in 3DNP metals processed at an elevated temperature near 873 K. A ring diffraction pattern proves the formation of BCC ligaments with various crystal orientations (inset in Figure 1c). The calculated lattice parameter (3.0544 Å) is analogous to the X-ray diffaction (XRD) result of the mature ligament. The ligament coarsened to 44 nm after 10 min of LMD at 1073 K (Figure 1d). The 3DNP HEA preserves its nanoscale features in severe conditions. The same BCC ring diffraction pattern implies that the parent FCC1 phase transforms rapidly into the BCC structure of ligaments when dealloying begins. The ligaments matured to 89 nm after 120 min of LMD at 1073 K (Figure 1e).

Most of ligaments consist of a few grain, and they form the polycrystalline 3DNP HEA scaffolds (Figure 1f). A high fraction of coincidence site lattice (CSL) boundaries (0.552 ± 0.078, the average value taken from three different areas) connotes the reducing the total energy by the formation of low energy grain boundary during phase transformation (Figure 1g). Crystal rotation among ligaments owing to the particular angles of CSL boudnaries results in the specific texture of crystal orientation (Figure S2, Supporting Information).

The compositions of the synthesized BCC ligaments inherit the compositions of the immiscible elements in their parent FCC phases (Table S1, Supporting Information). By energy-dispersive X-ray (EDX) analysis equipped in transmission electron microscopy (TEM), it is confirmed that the constituent elements are homogeneously distributed even in 10 nm ligament, and there is no segregation (Figure 1h). These compositional investigations satisfy the compositional high-entropy criterion of five major elements at concentrations ranging between 5 and 35 at%, suggesting that this new approach can develop 3DNP HEA. More importantly, the stability of BCC ligament can be judged from their compositions by analyizing valence electron concentration (VEC), which control the phase stability for FCC or BCC solid solution. The evaluated VEC of 8.80 (FCC1), 8.71 (FCC2), 5.15 (BCC1), and 4.95 (BCC2) agree with the VEC

criteria for FCC or BCC phase stability in HEAs; VEC < 6.87 for BCC, 6.87 ≤ VEC < 8.0 for FCC + BCC, and VEC ≥ 8.0 for FCC.[31]

Coarsening kinetics of 3DNP HEA is drastically minimized at elevated temperatures (**Figure 2**a,b). Using an Arrhenius-type equation on the diffusivity and ligament size,[32,33] the coarsening component, n, is determined to be 3.44–3.61, which is close to the kinetic parameter, ≈4, reflecting surface diffusion. Thus, surface diffusion governs the coarsening of the 3DNP HEA, as in the conventional porous metals.[33–36] Similar n values at different temperatures imply the invariable coarsening mechanism of 3DNP HEA. The temperature

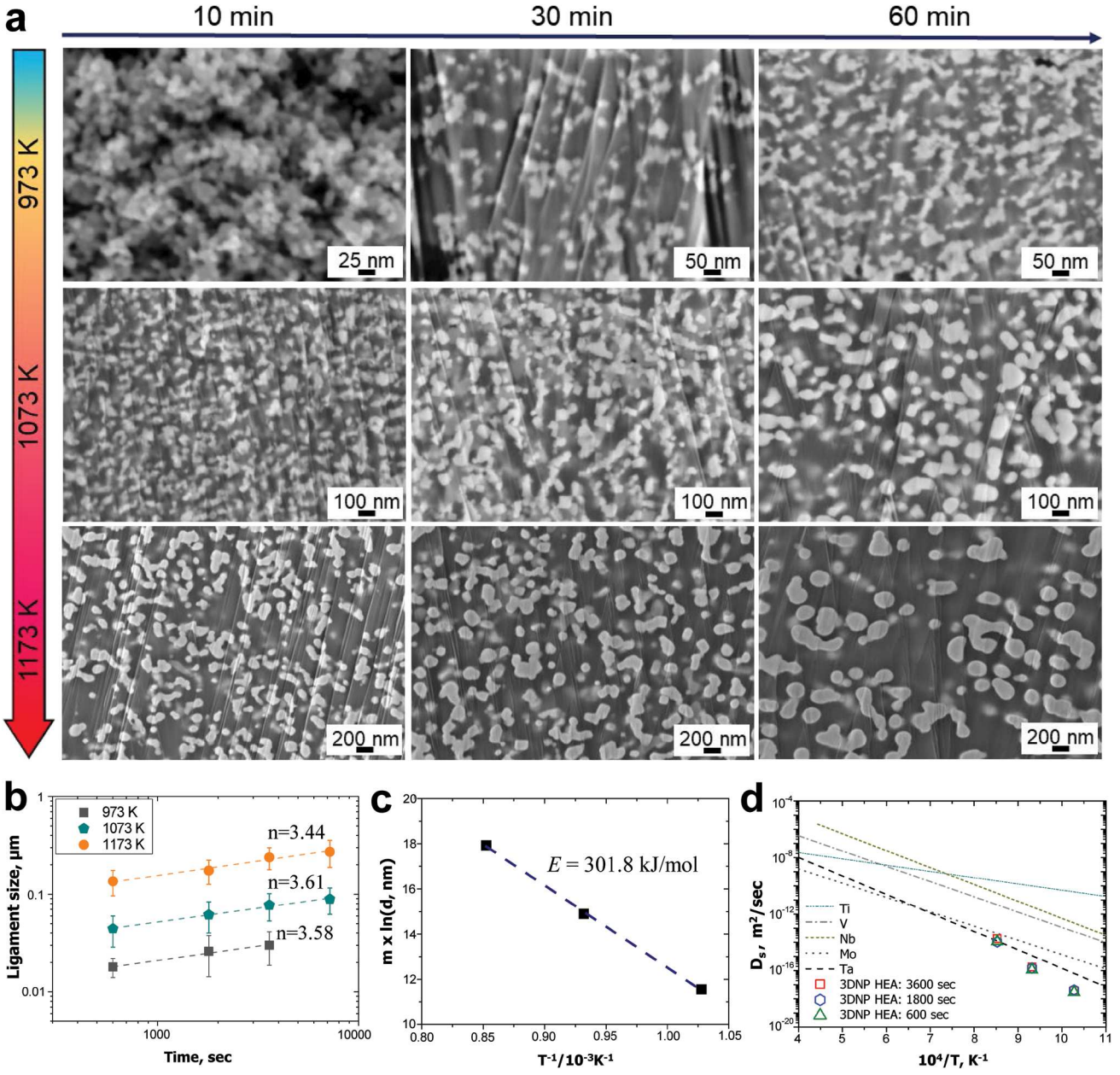

Figure 2. Kinetics of ligament coarsening and surface diffusivity of the 3DNP HEA. a) High-magnification FE-SEM images of 3DNP HEAs produced at 973 to 1173 K after dealloying for 10 to 60 min. b) Ligament size and distribution of the 3DNP HEA versus dealloying time at various temperatures. The relationship between dealloying time, t, and ligament size, d, can be expressed by a power function: $d^n = ktD$, where n is the coarsening component, k is a constant, and D is the surface diffusivity. The coarsening exponent, n, can be measured by plotting the ln[d(t)] versus ln t curve. Error bars denote the distribution of ligament sizes. c) Calculated activation energy for the coarsening of the 3DNP HEA. d) Estimated surface diffusivity of the 3DNP HEA compared with its constituent elements. The extrapolated lines of the constituent elements are obtained from the references of Ti,[41] V,[42] Mo,[43] Nb,[43] and Ta.[44] e) Illustration of the evolution of the 3DNP HEA during LMD. f) Specific surface areas measured with the BET method as a function of the ligament size. The lines correspond to the predictions of the analytic model $S = C/\rho d$. The inset shows the nitrogen adsorption/desorption curves for 3DNP HEAs with average ligament size ≈10 nm. The solid bulk density ρ is assumed to be 7.7 g cm^{-3} from the average atomic weight and radius of the constituent elements.

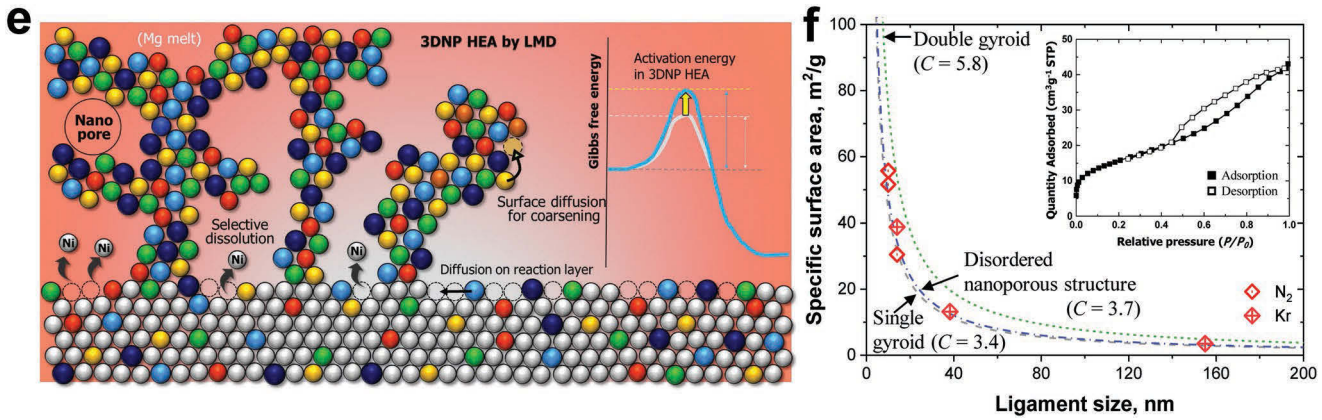

Figure 2. Continued.

dependence of the ligament size is represented by combining the power law of the coarsening component with an Arrhenius-type equation of diffusivity. Then, the activation energy for coarsening is calculated to be 301.8 kJ mol^{-1} (Figure 2c). Unlike the experimental result, the activation energies for surface diffusion of each element from the literature lead to a lower value of 192.9 kJ mol^{-1}, estimated using the rule of mixtures (ROM) (Table S2, Supporting Information).

Not only surface diffusion, there are other possible contributions on thermal coarsening of 3DNP materials such as bulk diffusion, surface chemistry, and phase separation.[37,38] In this study, the key factor leading to the exceptional stability can be determined to the slow surface diffusion of 3DNP HEA by eliminating other possible factors: 1) the coarsening parameter near 4 signifies a minor contribution of bulk diffusion, 2) the similar activation energies solid–vacuum and solid–liquid interfaces remove the surface chemistry effect, and 3) a single BCC phase is confirmed by SAED patterns.

Based on the surface-diffusion-based coarsening mechanism, the average surface diffusivity of HEA atoms can be estimated by the equation[33,39]

$$D_s = \frac{\mathrm{d}(t)^4\, kT}{32\gamma t a^4} \tag{1}$$

where k is the Boltzmann constant (1.3806×10^{-23} JK^{-1}), γ is the surface energy (2.306 Jm^{-2}, calculated by ROM using the values from literature[40]), t is the dealloying time, and a is the lattice parameter (3.2345×10^{-10} m measured by XRD) of the 3DNP HEA ligament. The evaluated average surface diffusivity is lower than that of Ta, which has the slowest diffusion kinetics among the constituent elements[41–44] (Figure 2d). Thus, the ultrastable nanostructure of 3DNP HEA results from the high activation energy for coarsening and the minimized surface diffusivity.

During the LMD process, the miscible element Ni is exclusively dissolved into the Mg melt, while the immiscible five elements forms an interconnected ligament structure with nanochannel of liquid melt, simultaneously (Figure 2e). A diffusion study by Tsai et al. gives persuasive evidence of the slower diffusion of HEAs.[23] Alloys with multiple principal elements have larger fluctuations in LPE than traditional alloys, providing many low-LPE sites that hinder atomic diffusion. On the other hand, other negative conclusions in recent articles in FCC HEAs make the sluggish diffusion phenomenon very controversial.[45–48] The five number of principal atoms do not guarantee an extra slugging effect, but a specific element possibly produces a deep potential wall, like Mn in CoCrFeMnNi alloy. Nevertheless, most of researchers found the slower diffusion of HEAs on a homologous temperature scale.[23,45,46] There are no applicable references on the diffusion behavior of refractory BCC HEAs. Therefore, a thorough study should be performed to clarify whether it is really sluggish diffusion due to low-LPE sites given by small atoms (schematic graph in Figure 2e, Ti or V in the current study) in HEA or just an unsophisticated effect of a particular element.

The exceptional stability against thermal coarsening results in high specific surface areas of 3DNP HEAs at elevated temperatures (Figure 2f). The measured specific surface areas are 55.7 (<10 nm), 38.8 (14 nm), and 3.6 (155 nm) m^2 g^{-1} depending on the ligament size. These are obtained following the analytical model proposed by Detsi et al.,[49] in which we use the dimensionless parameter $C = 3.7$ for disordered nanoporous structures in the equation $S = C/\rho d$; S is the specific surface area, ρ is the solid bulk density, and d is the ligament thickness. Furthermore, the adsorption/desorption isotherm curve corresponds to Type IV in the IUPAC classification[50] (inset in Figure 2f) when the ligament size is ≈10 nm. The hysteresis loop in the type IV isotherm is associated with capillary condensation in nanopores (<50 nm) at high P/P_0, and the type of isotherm is the same as that of nanoporous gold (NPG).[49] Thus, the isotherms confirm the presence of nanopores in 3DNP HEAs with structure similar to those of NPG.

A further important consideration is, the large fraction of CSL boundaries (Figure 1g) should work as pinning sites impeding atomic movements on the surface. On the contrary to chemical dealloying, phase transformations (here, FCC to BCC) occur during LMD based on an orientation relationship generating a high fraction of CSL boundaries.[51] Direct observation of the beneficial effects of twin boundary in stabilizing nanostructure of NPG has been reported by TEM.[8] Also, stabilized nanosteps by plana defects like stacking faults or twin boundary on nanoparticle Cu implicit the significant effect of CSL boudnary against thermal coarsening.[52] Thus, suppressed

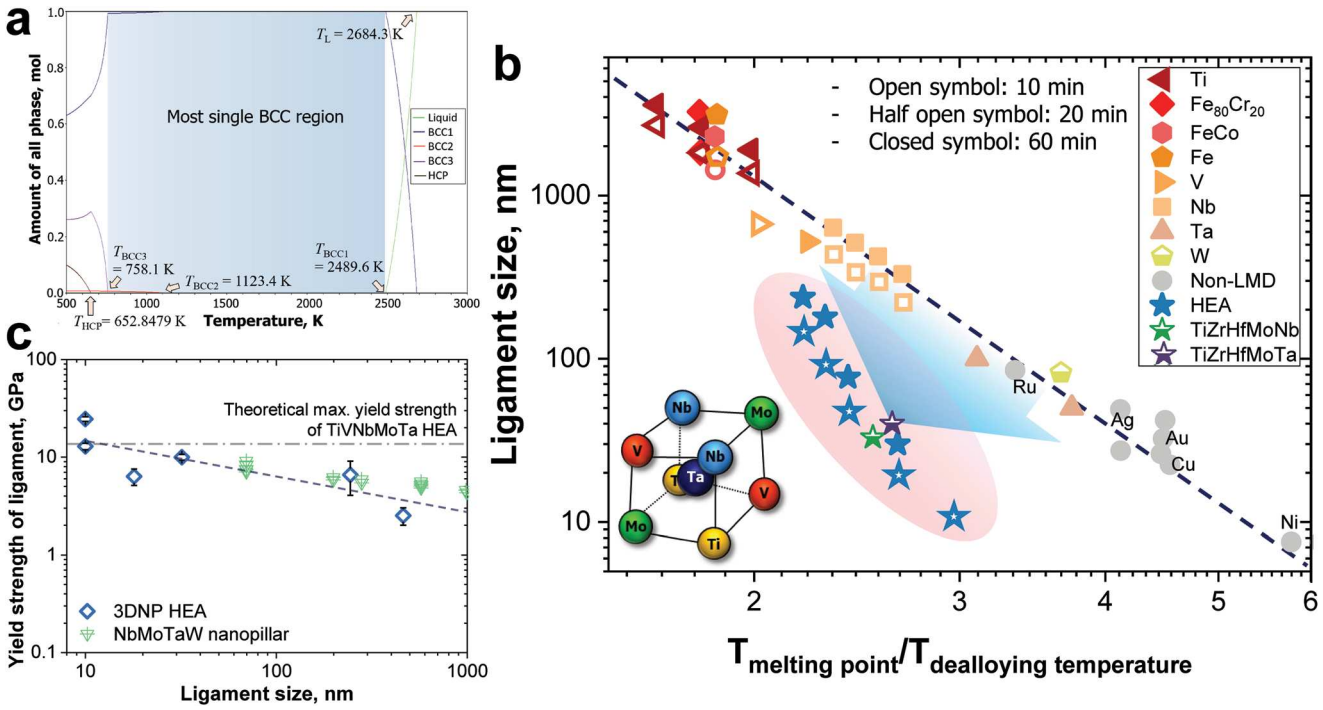

Figure 3. Thermal stability of 3DNP HEAs and preservation of physical property. a) Equilibrium phases and their fractions of the 3DNP HEA calculated as a function of temperature. b) Ligament size versus homologous temperature in conventional nano- and microporous materials and the 3DNP HEAs. Data points of Fe, FeCo, FeCr, Nb, and Ti are obtained from power-law fitting of $d^n = ktD$. The results of V, W, Ta, TiZrHfMoNb, and TiZrHfMoTa are used without fitting (Figure S3, Supporting Information). Non-LMD represents the nanoporous materials obtained by chemical dealloying;[2] the dealloying time is different from the LMD-based materials. c) Yield strength of the 3DNP HEA ligament and a NbMoTaW nanopillar[59] versus the ligament size/diameter of the pillar. The gray dashed-dotted line represents the theoretical maximum yield strength of TiVNbMoTa HEA. Error bars denote standard deviations.

coarsening in the 3DNP HEA should originate from the high fraction of secure CSL boundaries and the slow diffusion in multiprincipal elements.

Thermodynamic calculations were conducted to investigate the stability of the BCC phase and the melting point (**Figure 3**a). The results depict liquidus and solidus temperatures of ≈2684 and ≈2490 K, respectively, followed by a single BCC phase temperature down to 1123 K. Below 1123 to 758 K, the high temperature BCC crystal structure could partially transform to another BCC phase, but the amount of the second BCC phase is negligible. The thermodynamic study certifies the ligament of only single BCC phase and its melting temperature as 2584 K.

Chen and Sieradzki proposed that the stabilized steady-state ligament sizes at an ambient temperature of various nanoporous materials exhibit an empirical correlation with homologous temperature: $T_H = T_{298K}/T_{melting\ point}$.[1] Recently, McCue et al. expanded this correlation to LMD-processed porous materials by the modified homologous temperature ($T_H = T_{melting\ point}/T_{dealloying\ temperature}$) concerning the dealloying temperature.[2] Since the dealloying time also has strong influence on coarsening of LMD-based materials, it was fixed to 10, 20, or 60 min to clarify current analysis (Figure S3 of the Supporting Information for details). Pure and binary porous metals evidently follow the general relationship of ligament size versus homologous temperature in a log–log scale (Figure 3b). However, the linear relationship shifts down by one order of magnitude in smaller-size regime for the new 3DNP HEA. It is important to emphasize that ligament coarsening follows the power-law function; thus, the stabilized size regime of 3DNP HEA after 60 min cannot be achieved in conventional porous materials. The sharp slope of 3DNP HEAs in Figure 3b would be relevant with anomalous non-linear Arrhenius plots between ln D and $1/T$ in BCC transition pure metals and alloys.[53–56] The homogeneous 3DNP HEAs from a single phase precursor, which designed based on the composition of FCC 1 phase, were also successfully produced with their exceptional small sizes of ligament (Figure S4, Supporting Information). Moreover, different TiZrHfMoNb and TiZrHfMoTa 3DNP HEAs validate our high-entropy strategy (Figure 3b; Figure S3, Supporting Information). Thus, our new 3DNP HEA overcomes the universal effect of temperature on the coarsening of nanomaterials.

The major drawback of nanoporous materials is the physical property deterioration subsequently occurred by drastic coarsening. For example, coarsening of NPG continuously degrades its catalytic performance from 90% to 70% after 500 min at room temperature.[8] The yield strength of ligaments in 3DNP materials can reach the theoretical strength when the ligament size becomes a few nanometres.[7] Unfortunately, similar to their functional properties, their mechanical characteristics tend to dramatically deteriorate as ligaments coarsen. This study reveals the effectiveness of high-entropy design strategy to suppress the coarsening drawback by producing materials with excellent structural stability at elevated temperatures.

The yield strengths of 3DNP HEA ligaments were calculated with the adjusted Gibson and Ashby scaling model[57] of foam plasticity using nanoindentation (Figure 3c; Table S3, Supporting Information). This 3DNP HEA demonstrates a high yield strength of ligament close to the theoretical limit by reducing the size of ligament down to 10 nm. Such a high strength through dislocation starvation (so-called size-effect) has been reported in small-sized metallic systems[58] including NbMoTaW HEA nanopillars[59] and NPG.[7,60,61] Many nanoporous metallic materials are very brittle under tension because of their macroscopic structures, but nanoligaments show their intrinsic ductile behavior and high yield strengths under compressive stress. When the 3DNP ligament size becomes a few nanometers, the depleted dislocations and sources in nanoscale ligaments should lead to a high stress for nucleation of dislocation at free surfaces. Although there are some disparities between the current study and the literature due to different materials and experimental conditions, the role of outstanding stability of the 3DNP HEA is considered more important when assessing its physical properties in view of coarsening. Compared with general pure metals[62,63] or binary alloys,[64,65] 3DNP HEA shows a much slower coarsening rate and loss of desired 3DNP structure, thus, the porous structure of 3DNP HEA remains in the nanoscale regime after the same heat treatment. Consequently, the outstanding yield strength of ligaments in 3DNP HEA remains close to the theoretical strength ($G/2\pi$) after the subjection to elevated temperature.

The effort to overcome intrinsic thermal coarsening has led to the design of a new class of 3DNP materials via high-entropy strategy. By exploiting thermally activated coarsening at high temperatures, the exceptional stability of 3DNP material is achieved through implementation of slow surface diffusion obtained by high-entropy design. The empirical correlation of ligament size with homologous temperature for 3DNP HEA is shifted one order of magnitude toward smaller, and the stabilized nanoscale features of 3DNP HEA preserve its high yield strength of ligament despite exposure to severe conditions. These findings push toward a new generation of nanomaterials with excellent long-term performance.

Experimental Section

Precursor and 3DNP HEA Fabrication: The precursor alloy was produced from pure metals (99.99 at%) by arc melting under a purified argon atmosphere. The button-shaped ingot was turned over and remelted more than four times to ensure the homogeneity of its chemical composition. The Mg-10 at% Ca melt was prepared by induction heating under a purified helium atmosphere. An additional 10 at% Ca reduced the melting point below 873 K, and the relationships of miscibility between Ca and five HEA elements are similar with those of Mg. The precursor ingot was cut into a 1.5 mm thick plate, which was immersed in the melt. After dealloying, the Mg-rich phase was etched out in 3 M HNO_3 for 5 h.

Microstructure and Nanoindentation: The structure of the precursor alloy and 3DNP HEA was investigated by using XRD (Ultima IV, Rigaku, Tokyo, Japan) with Cu-Kα radiation, and its microstructure and composition were explored by using FE-SEM (Ultra 55, ZEISS, Oberkochen, Germany) coupled with EDX analysis (Quantax, Bruker, Billerica, MA, USA). The ligament size, pore size, porosity, and surface area were measured in ImageJ software, using FE-SEM images of the cross-sectional surface of the dealloyed plate, prepared by ion-milling (E-3500, Hitachi, Tokyo, Japan). The image analysis was performed on more than three images to guarantee its reliability. The nanoporous structures of 3DNP HEA were observed using a JEM-ARM200F (JEOL, Peabody, MA, USA). TEM samples were prepared using an FIB (Versa 3D, FEI, Hillsboro, OR, USA) or using thin ribbon-like powder precursors made by melt spinning. EBSD was conducted at an acceleration voltage of 15 keV in combination with an FE-SEM (Jeol 7100F, JEOL, Peabody, MA, USA). The step-size of the automatic scanning beam was 20 nm, and data points with a confidence index below 0.5 were eliminated. The specific surface area was calculated with the Brunauer–Emmett–Teller (BET) method. Nitrogen adsorption–desorption isotherms measured at 77 K to a relative pressure (P/P_0) of 0.995 by nitrogen physisorption on a BELSORP-maxII. For 3DNP HEAs with large ligaments (≥14 nm), Kr gas was used for low-surface-area analysis.

Thermodynamic calculations were conducted based on CALPHAD (CALculation of PHAse Diagram) scheme using commercial software (Thermo-Calc, 2019a) with the database for HEAs (TCHEA3: High Entropy Alloys v3.1). Specifically, equilibrium phases and their mole fractions were calculated as a function of temperature between 500 and 3000 K by every 50 K step after selecting the constituent elements of Ti, V, Nb, Ta, Mo, and Ni. As many as 63 phases including solid solutions and compounds were involved in the calculations where these default phases were selected automatically by designating the constituent elements. Condition definitions included pressure of 10^5 Pa and system size of unity in mole, and a $Ti_{13.29}V_{26.67}Nb_{19.91}Mo_{27.77}Ta_{12.16}Ni_{0.2}$ (at%) alloy.

The yield strength of ligaments in 3DNP HEA was calculated from direct load-controlled nanoindentation measurements by PI-85L (Hysitron, Minneapolis, MN, USA), in an FE-SEM (Helios Nanolab, FEI, USA), using a Berkovich tip. The sample surfaces were polished flat in parallel using ion-milling, and in situ FE-SEM allowed to select stable indenting positions without parent phase boundaries. The maximum load and loading rate were 5000 μN and 1000 μN s^{-1}, respectively. The holding time and unloading time were 5 s. Using a load–displacement curve, the hardness of the 3DNP HEA was calculated by the Oliver–Pharr method. The distance between indents was three-times larger than the size of indent. More than five indentations were averaged for an averaged hardness value (Figure S5, Supporting Information). The hardnesses obtained from the nanoindentation tests can be converted into the yield strength of the porous materials, because the yield strength equals the hardness in a porous structure due to the densification without constraint.[66] Also, the yield strength of the ligament (σ_{ys}) is given by the adjusted model[57] of foam plasticity originally developed by Gibson and Ashby.[67]

Supporting Information

Supporting Information is available from the Wiley Online Library or from the author.

Acknowledgements

This work was supported by Grant-in-Aid for Scientific Research on the innovation area "Science of New-Class of Materials Based on Elemental Multiplicity and Heterogeneity (Grant No. 18H05452)" from the Ministry of Education, Culture, Sports, Science and Technology (MEXT, Japan), by the International Collaboration Center Institute for Materials Research (ICC-IMR, Tohoku University), and by the German Science Foundation under the Leibniz Program (Grant No. MA 3333/13-1).

Conflict of Interest

The authors declare no conflict of interest.

Author Contributions

S.-H.J., I.V.O., and H.K. designed the research. S.-H.J. was the lead experimental scientist of the study and performed most of the experimental work. I.V.O. designed the material and conducted the proof of concept. W.-Y.P. performed the specific surface area measurements. J.W.B. and H.S.K. conducted the nanoindentation tests. Y.S., S.-H.J., and T.J.K. performed the TEM analysis. T.W. and H.K. contributed to the coarsening kinetics of the referenced porous materials. A.T. supported thermodynamic calculations. S.-H.J. wrote the manuscript with the contribution of I.V.O. All authors discussed the results and commented on the manuscript.

Keywords

liquid metal dealloying, nanoporous high-entropy alloys, size-dependent strength, thermal coarsening, thermodynamic calculation

[1] Q. Chen, K. Sieradzki, *Nat. Mater.* **2013**, *12*, 1102.
[2] I. McCue, A. Karma, J. Erlebacher, *MRS Bull.* **2018**, *43*, 27.
[3] L.-Y. Chen, J.-S. Yu, T. Fujita, M.-W. Chen, *Adv. Funct. Mater.* **2009**, *19*, 1221.
[4] C. Xu, J. Su, X. Xu, P. Liu, H. Zhao, F. Tian, Y. Ding, *J. Am. Chem. Soc.* **2007**, *129*, 42.
[5] X. Zhou, W. Xu, G. Liu, D. Panda, P. Chen, *J. Am. Chem. Soc.* **2010**, *132*, 138.
[6] L. H. Qian, X. Q. Yan, T. Fujita, A. Inoue, M. W. Chen, *Appl. Phys. Lett.* **2007**, *90*, 153120.
[7] J. Biener, A. M. Hodge, J. R. Hayes, C. A. Volkert, L. A. Zepeda-Ruiz, A. V. Hamza, F. F. Abraham, *Nano Lett.* **2006**, *6*, 2379.
[8] T. Fujita, T. Tokunaga, L. Zhang, D. Li, L. Chen, S. Arai, Y. Yamamoto, A. Hirata, N. Tanaka, Y. Ding, M. Chen, *Nano Lett.* **2014**, *14*, 1172.
[9] J.-W. Yeh, S.-K. Chen, S.-J. Lin, J.-Y. Gan, T.-S. Chin, T.-T. Shun, C.-H. Tsau, S.-Y. Chang, *Adv. Eng. Mater.* **2004**, *6*, 299.
[10] D. B. Miracle, O. N. Senkov, *Acta Mater.* **2017**, *122*, 448.
[11] O. N. Senkov, G. B. Wilks, J. M. Scott, D. B. Miracle, *Intermetallics* **2011**, *19*, 698.
[12] P. Shi, W. Ren, T. Zheng, Z. Ren, X. Hou, J. Peng, P. Hu, Y. Gao, Y. Zhong, P. K. Liaw, *Nat. Commun.* **2019**, *10*, 489.
[13] C. Lee, G. Song, M. C. Gao, R. Feng, P. Chen, J. Brechtl, Y. Chen, K. An, W. Guo, J. D. Poplawsky, S. Li, A. T. Samaei, W. Chen, A. Hu, H. Choo, P. K. Liaw, *Acta Mater.* **2018**, *160*, 158.
[14] Z. J. Zhang, M. M. Mao, J. Wang, B. Gludovatz, Z. Zhang, S. X. Mao, E. P. George, Q. Yu, R. O. Ritchie, *Nat. Commun.* **2015**, *6*, 10143.
[15] Z. Tang, T. Yuan, C.-W. Tsai, J.-W. Yeh, C. D. Lundin, P. K. Liaw, *Acta Mater.* **2015**, *99*, 247.
[16] S. Chen, W. Li, X. Xie, J. Brechtl, B. Chen, P. Li, G. Zhao, F. Yang, J. Qiao, P. K. Liaw, *J. Alloys Compd.* **2018**, *752*, 464.
[17] Y. Qiu, S. Thoma, D. Fabijanic, A. J. Barlow, H. L. Fraser, N. Birbilis, *Mater. Des.* **2019**, *170*, 107698.
[18] Y. Shi, B. Yang, X. Xie, J. Brechtl, K. A. Dahmen, P. K. Liaw, *Corros. Sci.* **2017**, *119*, 33.
[19] Y. L. Chou, J. W. Yeh, H. C. Shih, *Corros. Sci.* **2010**, *52*, 2571.
[20] N. A. P. K. Kumar, C. Li, K. J. Leonard, H. Bei, S. J. Zinkle, *Acta Mater.* **2016**, *113*, 230.
[21] P. P. Bhattacharjee, G. D. Sathiaraj, M. Zaid, J. R. Gatti, C. Lee, C.-W. Tsai, J.-W. Yeh, *J. Alloys Compd.* **2014**, *587*, 544.
[22] C.-S. Wu, P.-H. Tsai, C.-M. Kuo, C.-W. Tsai, *Entropy* **2018**, *20*, 967.
[23] K. Y. Tsai, M. H. Tsai, J. W. Yeh, *Acta Mater.* **2013**, *61*, 4887.
[24] T. Wada, K. Yubuta, A. Inoue, H. Kato, *Mater. Lett.* **2011**, *65*, 1076.
[25] P.-A. Geslin, I. McCue, B. Gaskey, J. Erlebacher, A. Karma, *Nat. Commun.* **2015**, *6*, 8887.
[26] T. Wada, T. Ichitsubo, K. Yubuta, H. Segawa, H. Yoshida, H. Kato, *Nano Lett.* **2014**, *14*, 4505.
[27] I. V. Okulov, J. Weissmüller, J. Markmann, *Sci. Rep.* **2017**, *7*, 20.
[28] S.-H. Joo, T. Wada, H. Kato, *Mater. Des.* **2019**, *180*, 107908.
[29] S.-H. Joo, K. Yubuta, H. Kato, *Scr. Mater.* **2020**, *177*, 38.
[30] I. V. Okulov, A.V. Okulov, I. V. Soldatov, B. Luthringer, R. Willumeit-Römer, T. Wada, H. Kato, J. Weissmüller, J. Markmann, *Mater. Sci. Eng., C* **2018**, *88*, 95.
[31] S. Guo, C. Ng, J. Lu, C. T. Liu, *J. Appl. Phys.* **2011**, *109*, 103505.
[32] I. McCue, B. Gaskey, P.-A. Geslin, A. Karma, J. Erlebacher, *Acta Mater.* **2016**, *115*, 10.
[33] L. H. Qian, M. W. Chen, *Appl. Phys. Lett.* **2007**, *91*, 083105.
[34] T. Wada, H. Kato, *Scr. Mater.* **2013**, *68*, 723.
[35] J. Erlebacher, *Phys. Rev. Lett.* **2011**, *106*, 225504.
[36] Y. Ding, Y. J. Kim, J. Erlebacher, *Adv. Mater.* **2004**, *16*, 1897.
[37] H. Rösner, S. Parida, D. Kramer, C. A. Volkert, J. Weissmüller, *Adv. Eng. Mater.* **2007**, *9*. 535.
[38] J. Biener, A. Wittstock, M. M. Biener, T. Nowitzki, A. V. Hamaza, M. Baeumer, *Langmuir* **2010**, *26*, 13736.
[39] G. Andreasen, M. Nazzarro, J. Ramirez, R. C. Salvarezza, A. J. Arvia, *J. Electrochem. Soc.* **1996**, *143*, 466.
[40] W. R. Tyson, W. A. Miller, *Surf. Sci.* **1977**, *62*, 267.
[41] A. M. Dabrowski, T. Biernat, J. Beben, W. Gubernator, *Acta Phys. Pol. A* **1997**, *91*, 1091.
[42] J. M. Yu, R. Trivedi, *Surf. Sci.* **1983**, *125*, 396.
[43] J. A. Clum, *Metall. Trans.* **1973**, *4*, 1763.
[44] S. Hok, M. Drechsler, *Surf. Sci. Lett.* **1981**, *107*, L362.
[45] J. Dabrowa, M. Zajusz, W. Kucza, G. Cieślak, K. Berent, T. Czeppe, T. Kulik, M. Danielewski, *J. Alloys Compd.* **2019**, *783*, 193.
[46] J. Kottke, M. Laurent-Brocq, A. Fareed, D. Gaetner, L. Perrière, Ł. Rogal, S. V. Divinski, G. Wilde, *Scr. Mater.* **2019**, *159*, 94.
[47] W. Kucza, J. Dabrowa, G. Cieślak, K. Berent, T. Kulik, M. Danielewski, *J. Alloys Compd.* **2018**, *731*, 920.
[48] C. Zhang, F. Zhang, K. Jin, H. Bei, S. Chen, W. Cao, J. Zhu, D. Lv, *J. Phase Equilib. Diffus.* **2017**, *38*, 434.
[49] E. Detsi, E. De Jong, A. Zinchenko, Z. Vuković, I. Vuković, S. Punzhin, K. Loos, G. ten Brinke, H. A. De Raedt, P. R. Onck, J. T. M. De Hosson, *Acta Mater.* **2011**, *59*, 7488.
[50] M. Thommes, *Chem. Ing. Tech.* **2010**, *82*, 1059.
[51] S.-H. Joo, H. Kato, *Mater. Des.* **2020**, *185*, 108271.
[52] M. Behrens, F. Studt, I. Kasatkin, S. Kühl, M. Hävecker, F. Abild-Pedersen, S. Zander, F. Girgsdies, P. Kurr, B.-L. Kniep, M. Tovar, R. W. Fischer, J. K. Nørskov, R. Schlögl, *Science* **2012**, *336*, 893.
[53] J. M. Sanchez, D. de Fontaine, *Phys. Rev. Lett.* **1975**, *35*, 227.
[54] J. F. Murdock, C. J. McHargue, *Acta Metall.* **1968**, *16*, 493.
[55] R. F. Peart, D. H. Tomlin, *Acta Metall.* **1962**, *10*, 123.
[56] J. Pelleg, *Phys. Status Solidi A* **1995**, *147*, 361.
[57] S. S. R. Saane, K. R. Mangipudi, K. U. Loos, J. Th. M. De Hosson, P. R. Onck, *J. Mech. Phys. Solids* **2014**, *66*, 1.
[58] J. R. Greer, J. Th. M. De Hosson, *Prog. Mater. Sci.* **2011**, *56*, 654.
[59] Y. Zou, H. Ma, R. Spolenak, *Nat. Commun.* **2015**, *6*, 7748.
[60] A. M. Hodge, J. Biener, J. R. Hayaes, P. M. Bythrow, C. A. Volkert, A. V. Hamza, *Acta Mater.* **2007**, *55*, 1343.
[61] M. Hakamada, M. Mabuchi, *Scr. Mater.* **2007**, *56*, 1003.
[62] I. V. Okulov, P.-A. Geslin, I. V. Soldatov, H. Ovri, S.-H. Joo, H. Kato, *Scr. Mater.* **2019**, *163*, 133.

[63] I. V. Okulov, S. V. Lamaka, T. Wada, K. Yubuta, M. L. Zheludkevich, J. Weissmüller, J. Markmann, H. Kato, *Nano Res.* **2018**, *11*, 6428.
[64] I. V. Okulov, A. V. Okulov, A. S. Volegov, J. Markmann, *Scr. Mater.* **2018**, *154*, 68.
[65] A. V. Okulov, A. V. Volegov, J. Weissmüller, J. Markmann, I. V. Okulov, *Scr. Mater.* **2018**, *146*, 290.
[66] A. C. Fischer-Cripps, *Nanoindentation*, Springer, New York **2002**.
[67] L. J. Gibson, M. F. Ashby, *Cellular Solids: Structure and Properties*, 2nd ed., Cambridge University Press, UK **1997**.